Journal of Applied Electrochemistry **29**: 1111–1118, 1999.

An integrated flow reactor-membrane filtration system for heterogeneous photocatalysis. Part II: Experiments on the ultrafiltration unit and combined operation

K. SOPAJAREE[1], S.A. QASIM[1], S. BASAK[2] and K. RAJESHWAR[2]*
[1]*Department of Civil and Environmental Engineering; and*
[2]*Department of Chemistry and Biochemistry, The University of Texas at Arlington, Arlington, Texas 76019, USA (*author for correspondence)*

Received 17 February 1999; accepted in revised form 23 February 1999

Key words: dye photooxidation, titanium dioxide, total organic carbon

Abstract

A batch-recirculated photoreactor was combined with a hollow-fibre membrane ultrafiltration (UF) unit for heterogeneous photocatalysis applications. This paper focuses on the operation and modelling of the UF process component and on the performance of the integrated photoreactor–UF process assembly. Methylene blue and titanium dioxide (Degussa P-25) were used as the test pollutant and photocatalyst, respectively. The influence of cross-flow velocity, transmembrane pressure, and TiO_2 dose on the permeate flux through the hollow fibre membrane is described. These data are modelled on the basis of concentration polarization and gel layer formation at the membrane surface/feed slurry boundary. The operation of the integrated photoreactor–UF assembly over ten repeat cycles is described. Photocatalyst separation was complete as gauged by nephelometric turbidity measurements. However, a systematic degradation in the photocatalyst performance was noted with each repeat cycle. Dynamic laser light scattering data are consistent with agglomeration of the TiO_2 particles as a result of the UF process, and suggest a possible factor in the degraded photocatalytic activity. Possible solutions to this problem are finally presented.

1. Introduction

This study explores the feasibility of combining a batch-recirculated photoreactor with a hollow-fibre membrane ultrafiltration (UF) unit for heterogeneous photocatalysis applications. The companion paper [1] described the influence of several experimental variables (including substrate concentration, photocatalyst dose, recirculation flow rate, solution pH) on the photocatalytic reaction rate as monitored spectrophotometrically. This paper further builds on this concept, now focusing on the UF process component; it also describes the combined operation of the integrated photoreactor–UF process assembly. As in Part I of this study, methylene blue (MB) and titanium dioxide (Degussa P-25) were used as the test pollutant and photocatalyst, respectively.

The UF configuration adopted in the present study utilized a hollow-fibre membrane cartridge available commercially. The module consists of an array of narrow-bore (self-supported) fibres with a dense skin layer that affords permselectivity and a more open matrix to provide structural integrity. The cartridge is equipped with a feed inlet, a retentate outlet, and permeate ports. The UF process was operated in the cross-flow mode [2]. In a functional sense, the integrated system serves not only to recover the purified water from the photocatalyst suspension but also to recycle the photocatalyst for processing a fresh feed.

In this paper, we examine the influence of various parameters such as the TiO_2 dose, transmembrane pressure, and recirculation rate on the permeate flux through the UF membrane and interpret the results within the framework of the gel layer model for membrane filtration processes [2, 3]. We also describe the operation of the integrated system for ten repeat cycles. In each cycle, the MB solution was first treated in the photoreactor and the treated water plus the photocatalyst slurry were then routed to the UF unit wherein the TiO_2 particles were separated using a hollow-fibre membrane filter. The TiO_2 particles were then recycled back into the photoreactor. Although complete separation of the TiO_2 particles from the treated dye stream was noted, there was a systematic degradation in the photocatalyst performance with each repeat cycle. This trend was traced to agglomeration of the TiO_2 particles caused by the UF process. Finally, possible solutions to this potential problem are presented.

2. Experimental details

2.1. *UF unit and associated parameters*

Figure 1 contains a schematic diagram of the hollow-fibre membrane UF unit employed in this study. The hollow-fibre membrane cartridge was obtained from A/G Technology Corporation, Needham, Massachusetts. The characteristics of the particular cartridge used (UFP-100-E-3A) are listed in Table 1. The fibre length was 0.337 m.

A variable-speed peristaltic pump (Masterflex PRP-3) was used to circulate the solutions in the UF system. The key hydrodynamic parameters influencing permeate flux through the membrane are the transmembrane pressure (ΔP) and the shear rate [3] which in turn depends on the cross-flow velocity. Transmembrane pressure is defined as

$$\Delta P = \left(\frac{P_{\text{in}} + P_{\text{out}}}{2}\right) - P_{\text{permeate}} \tag{1}$$

In Equation 1, the subscripts 'in,' 'out,' and 'permeate' denote various locations in the unit, namely, inlet of the membrane cartridge, outlet of the membrane cartridge and outlet of the permeate port, respectively. This parameter was controlled in the present assembly by the back-pressure needle valve (P2) placed in the retentate line (Figure 1). The cross-flow velocity (or shear rate) was controlled by adjusting the pump speed (i.e., the recirculation rate).

Considerations of the volumetric flow rate (Q), the shear rate, and the Reynolds number showed that the flow was laminar at all the flow velocities relevant to this study. However, as discussed later, the shear rate strongly influences the concentration polarization and/or the gel layer at the membrane surface. An increase in the shear rate usually results in a concomitant increase in the permeate flux. The permeate flux was determined by measuring the time taken to reach a predetermined permeate volume (0.8 dm^3). Prior to each run, the permeate flux for pure water was measured to determine the initial permeability of the membrane. At the end of each run, the system was flushed at a high circulation velocity with the permeate valve closed to remove the deposited TiO_2 particles from the membrane surface. Backflush was applied with clean water until the initial permeability had been regained.

Table 1. Characteristics of the hollow-fibre membrane used in this study*

Hollow-fibre material	polysulphone
Inner diameter	1 mm
Thickness of membrane	
Dense layer	0.5–1 μm
Porous support	200 μm
Molecular weight cut-off	100 000 Da
Effective area	0.007 m^2
Number of fibres	12
Porosity	
Dense layer	10%
Support layer	80%

* Data provided by A/G Technology Corporation

The nominal pore size of the hollow fibre membrane used in this study may be estimated by the Hagen–Poiseuille equation [2–4]:

$$r_{\text{p}} = \left(\frac{8J\eta\ell}{\varepsilon\Delta P}\right)^{1/2} \tag{2}$$

In Equation 2, r_{p} is the capillary radius (with the porous UF membrane modelled as consisting of straight cylindrical capillaries [5], J is the permeate flux, ℓ is the membrane thickness, ε is the membrane porosity and η is

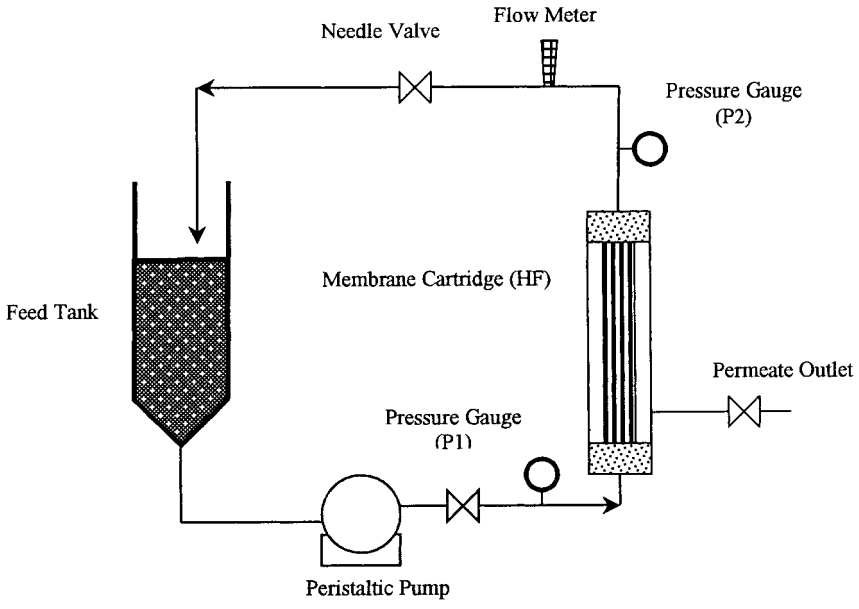

Fig. 1. Schematic diagram of the hollow-fibre membrane UF unit.

the fluid viscosity. Using Equation 2, pore sizes were estimated at different transmembrane pressures (ΔP) and were found to be 9.5 ± 0.3 nm.

2.2. *Integrated photoreactor–UF unit operation*

A typical experimental sequence using the integrated system (depicted in Figure 1 [1]) follows:

(i) Add 1 g dm^{-3} TiO_2 into the MB solution and mix by recirculating at 4.80 dm^3 min^{-1} for 20 min.
(ii) Take 5 cm^3 aliquots of solution to study the effect of adsorption of MB on the TiO_2 surface (cf. Part I of this series [1]).
(iii) Turn on the black u.v. light and circulate the solution through the photoreactor for 35 min.
(iv) Turn off the light and collect 5 cm^3 of solution.
(v) Begin filtration of the solution by turning on the pump at the membrane unit. Maintain cross-flow velocity at 2.56 m s^{-1} and a range of transmembrane pressures from 68.8 to 103.2 kPa.
(vi) Terminate the filtration when 0.8 dm^3 of permeate volume has been collected. Measure the turbidity, the total organic carbon (TOC), and the MB content of the collected permeate volume.
(vii) Apply a high cross-flow velocity to retentate for 5 min to route the TiO_2 'cake' to the photocatalytic reactor.
(viii) Start another run by adding enough volume of MB solution and additional TiO_2 to make up for losses during sampling.

Air was supplied to the feed tank through an air flow controller and a sand diffuser. The circulation rate in all experiments was 3.24 dm^3 min^{-1}. Air was continuously supplied at a rate of 1 dm^3 min^{-1} to provide O_2 (for the photocatalytic reaction) and to mix the solutions.

Solution samples were collected at four stages of each run: (a) at the beginning of the experiment; (b) after equilibration with TiO_2 in the dark; (c) after photocatalysis; and (d) after filtration in the UF membrane unit. Sampling details were given earlier [1]. The MB content of the solutions was determined spectrophotometrically as discussed earlier [1]. For TOC analysis, the samples were stored in amber glass bottles with Teflon-lined caps and the solutions were kept at pH < 2 by adding HCl. The TOC analyser at the Water Utilities Department, City of Arlington, Texas, was used.

2.3. *Photocatalyst particle size distribution, solution turbidity and other details*

The initial size distribution of the Degussa P-25 TiO_2 particles used in this study was determined by dynamic laser light scattering [6] using a Brookhaven Corporation (model B1-200) SM apparatus. The nominal particle size range in ten random trials varied from 100 to 1000 nm with a predominantly bimodal distribution peaking at ~380 nm and 600–800 nm (see below).

The effectiveness of the UF process for photocatalyst separation was assessed by water turbidity measurements [7]. The turbidity was measured using a Hach 2100 portable turbidimeter. Calibration experiments were run to relate the solution turbidity (in nephelometric turbidity units, NTU) to the TiO_2 dose. Deionized water was used as the blank in these tests. Regression analyses of these data yield the following expression:

$$\text{Turbidity} = 0.26 + 5270\,D \tag{3}$$

with a correlation coefficient of 0.9985. In Equation 3, D is the TiO_2 dose in g dm^{-3}.

Other details on the chemicals and the irradiation source were given in the companion paper [1].

3. Results and discussion

3.1. *Permeate flux through the UF membrane and its dependence on various process variables*

Figure 2 contains data for pure water; (a) shows the permeate flux (J) as a function of time with the transmembrane pressure (ΔP) as parameter, and (b)

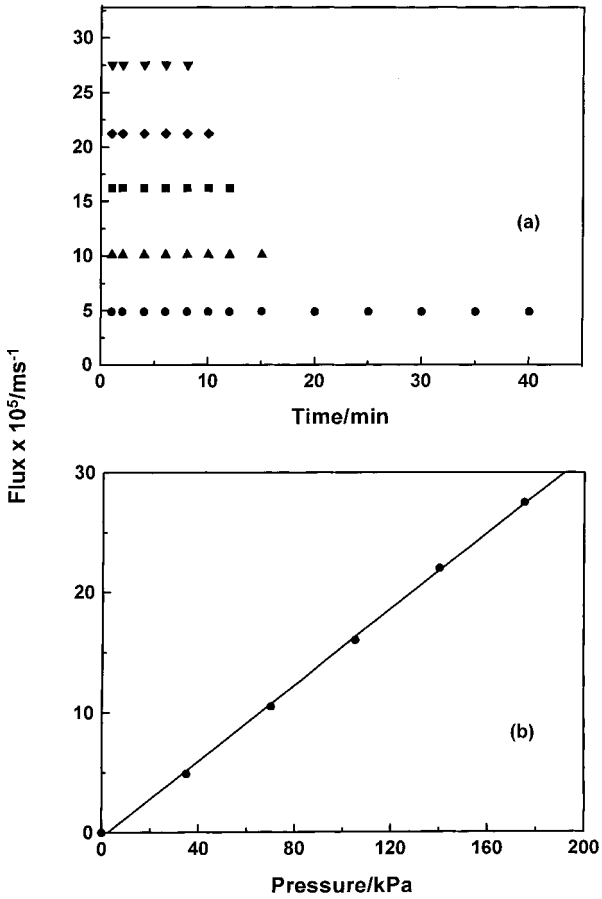

Fig. 2. (a) Dependence of permeate flux on time for pure water with the transmembrane pressure (in kPa) as parameter: (●) 34.4, (▲) 68.8, (■) 103.2, (◆) 137.6 and (▼) 172.0. (b) Plot of the flux against the transmembrane pressure constructed from the data in (a). Solid line is a least-squares fit of the data points.

contains the corresponding plot of J against ΔP. The two parameters are related via the expression [3, 8]:

$$J = \Delta P/\eta R_m \quad (4)$$

In Equation 4, $L_p = 1/\eta R_m$ is the hydraulic permeability and R_m is the hydraulic resistance of the membrane. The slope of the straight line in Figure 2(b) yields a value of L_p of 1.573×10^{-9} m Pa^{-1} s^{-1}. With a value for η of water of 1000 μPa s (at 25 °C), R_m is calculated to be 6.36×10^{11} m^{-1}.

The data in Figure 2 are diagnostic of the fact that the structural integrity of the hollow-fibre membrane is maintained at these transmembrane pressures for the duration of the experiment. It must also be noted that the permeate flux for pure water is independent of the shear rate (or cross-flow velocity) since there is no other resistance due to a polarization or gel layer. This contrasts with the TiO_2 aqueous slurries to be discussed next.

Figure 3 contains the corresponding data for a 1 g dm^{-3} TiO_2 slurry. The data in Figure 3 correspond to a constant cross-flow velocity of 0.97 m s^{-1}. Contrasting with the behaviour for pure water in Figure 2(a), the permeate flux exhibits an abrupt decrease with time and then attains a plateau after about 10 min of filtration (Figure 3(a)). This decrease is diagnostic of the buildup of a polarization/gel layer at the membrane surface (see below).

Figure 3(b) contains plots of the steady flux with ΔP. The data for pure water from Figure 2(b) are also shown for direct comparison. The systematic diminution in the permeate flux (relative to pure water) is another manifestation of the polarization/gel layer build-up. Simply put, the latter results in an effective decrease in the driving-force because of osmotic back-pressure and an increase in the total resistance of the membrane. However, the permeate flux increases with an increase in the cross-flow velocity (u) because of the removal of the polarization/gel layer at high shear rates.

Figure 4(a) shows the dependence of J on ΔP with the TiO_2 dose as parameter. The flux systematically decreases as the photocatalyst dose increases. Stated in different terms, the rate of increase of J with ΔP slows with increasing TiO_2 dose in the slurry feed. Analysis of

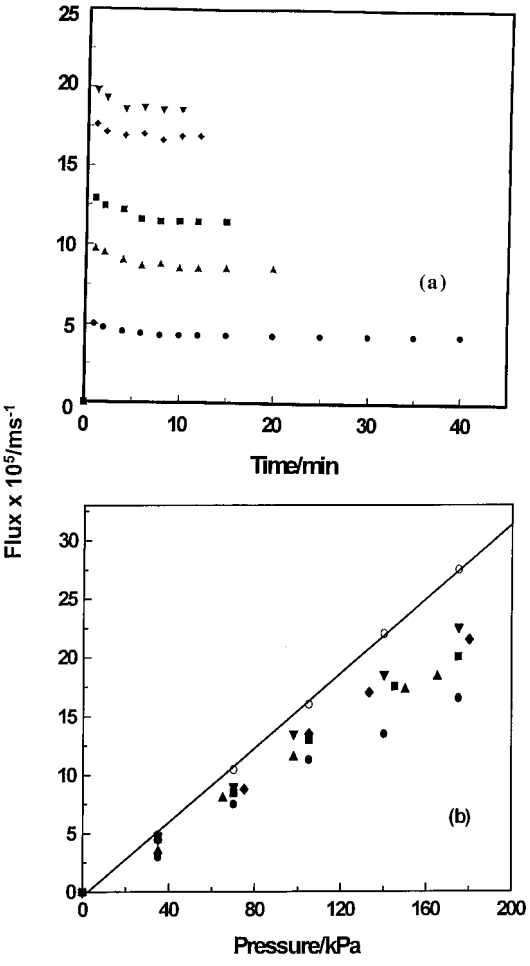

Fig. 3. (a) As in Figure 2(a) but for a 1 g dm^{-3} TiO_2 slurry at a constant cross-flow velocity of 0.97 m s^{-1}: (●) 34.4, (▲) 65.4, (■) 96.3, (◆) 147.9 and (▼) 165.1. (b) As in Figure 2(b) but for the solution in Figure 3(a) and with the cross-flow velocity (u) as a parameter. Plot for pure water from Figure 2(b) is also shown for comparison. Values for u (in m s^{-1}) are: (●) 0.54, (▲) 0.97, (■) 1.50, (◆) 2.03 and (▼) 2.92.

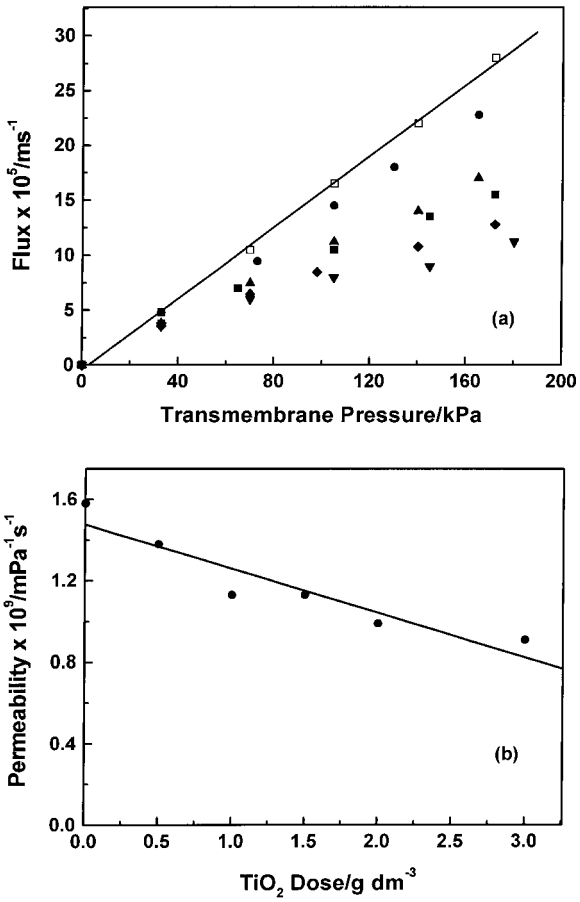

Fig. 4. (a) As in Figure 3(b) but with the TiO_2 dose as a parameter. A plot for pure water from Figure 2(b) is also shown for comparison. Cross-flow velocity was kept constant at 0.54 m s^{-1}. Values for the TiO_2 dose (in g dm^{-3}) are: (●) 0.5, (▲) 1.0, (■) 1.5, (◆) 2.0 and (▼) 3.0. (b) Plot of the hydraulic permeability against TiO_2 dose constructed from the data in Figure 4(a). Solid line is a least-squares fit.

the initial slopes in Figure 4(a) again affords estimates of the hydraulic permeability, L_p. This parameter shows a systematic decrease with the TiO_2 dose as illustrated in Figure 4(b).

3.2. *UF process modelling considerations*

Membranes can develop resistance to fluid flow during the filtration process for a variety of reasons as schematized in Figure 5(a). Under such conditions, the permeate flux will be a function of time (as exemplified by the data in Figure 3(a)) until a steady-state situation develops. On the other hand, in clean water, the only resistance is that presented by the membrane itself, R_m. Since R_m is constant, the permeate flux will be independent of time (Figure 2(a)) and a plot of J against ΔP will be linear whence a value for R_m may be calculated (Equation 4).

In a slurry feed, the three major process resistances are due to pore blocking, gel-layer formation, and concentration polarization as illustrated in Figure 5(a). The gel layer refers to the situation when the concentration of the suspended particles at the membrane surface/solution becomes very high [3, 9, 10]. This build-up also generates diffusive mass transport back to the bulk of the feed as illustrated in Figure 5(b). At steady state, the forward and back flow components balance one another. This is the concentration polarization situation. Each of these process components has an associated resistance (Figure 5(a)) such that the membrane resistance in Equation 4 must be replaced by an effective resistance R given by $R = R_m + R_f$, where R_f is the resistance to the fouling processes discussed above. (In a steady-state condition, the time dependence of R_f may be ignored.) In contrast to Equation 4, it must be noted that R is a function of ΔP such that a plot of J against ΔP no longer is constrained to be linear. The influence of the gel layer may be explicitly considered by the following expression [3]:

$$J = \frac{\Delta P}{\eta R + (\Delta P / J_g)} \tag{5}$$

In Equation 5, J_g is the limiting flux through the gel layer (i.e., as $\Delta P \to \infty$, $J \to J_g$) [4]. Pore blocking is considered to contribute negligibly in the present case since the nominal TiO_2 particle size is 10–100 times greater than the membrane pore diameter.

The polarization/gel layer model thus can be analyzed by a reciprocal plot according to the expression:

$$\frac{1}{J} = \frac{1}{J_g} + \frac{\eta R}{\Delta P} \tag{6}$$

Figures 6 and 7 contain such plots with the cross-flow velocity (u) and TiO_2 dose as parameters, respectively. These plots were constructed from the data presented earlier in Figures 3 and 4. The good linearity of these plots is taken to support the essential validity of the

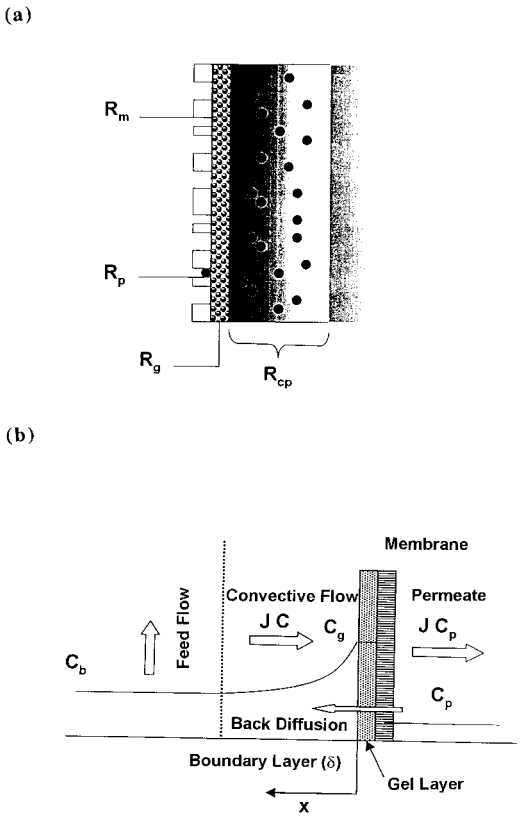

Fig. 5. (a) Schematic diagram showing formation of the gel layer and the concentration polarization layer. The R's are the various resistance components, R_m is the membrane resistance, and the subscripts 'p', 'g', and 'cp' denote pore-blocking, gel-layer, and concentration polarization, respectively (refer to text). (b) Schematic diagram of the mass-transport dynamics in the present UF unit. J is the flux and the C's are concentration terms with the subscripts 'b' and 'p' denoting bulk and permeate, respectively. Subscript 'g' has the same significance as in Figure 5(a).

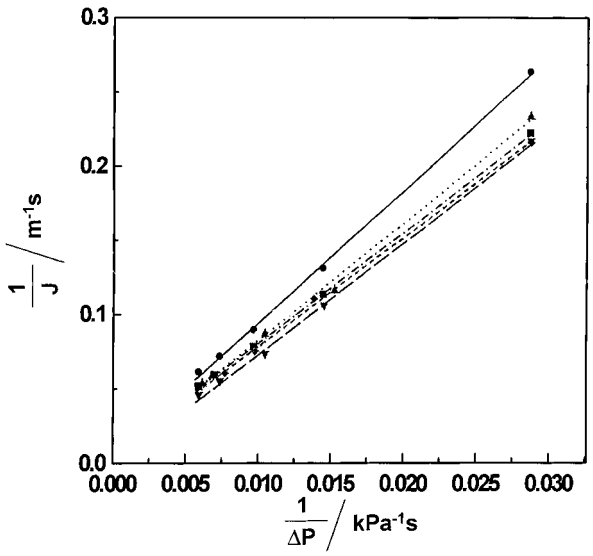

Fig. 6. Reciprocal plot of $1/J$ against $1/\Delta P$ (Equation 6) with the cross-flow velocity (in m s^{-1}) as a parameter: (●) 0.54, (▲) 0.97, (■) 1.50, (◆) 2.03, and (▼) 2.92. Lines are least-squares fits. Data are for a 1 g dm^{-3} TiO_2 slurry.

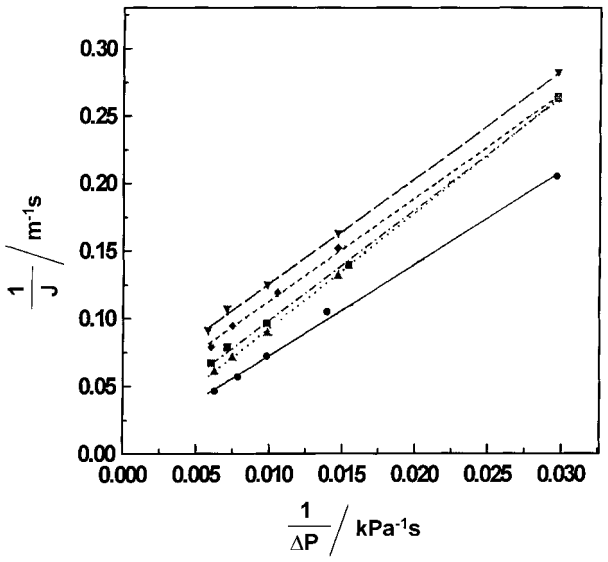

Fig. 7. As in Figure 6 but with the TiO_2 dose (in g dm^{-3}) as parameter: (●) 0.5, (▲) 1.0, (■) 1.5, (◆) 2.0 and (▼) 3.0.

polarization/gel layer model for the TiO_2 UF process. Values for the parameters R and J_g obtained from the slopes and intercepts of these reciprocal plots are given in Tables 2 and 3, respectively.

The R values are in the 6.36×10^{11} m^{-1} to 8.47×10^{11} m^{-1} range; they are only weakly dependent on the two parameters, u and TiO_2 dose. The limiting flux through the gel layer (J_g) also is reasonably independent of u, but it decreases systematically with increasing TiO_2 dose.

The effect of u and ΔP on the deposition of TiO_2 on the membrane surface (i.e., gel formation) can be observed by measuring the residual TiO_2 concentration in the bulk solution before and after filtration. These experiments were run without any back flush applied to the membrane (Section 2). An initial TiO_2 dose of 1 g dm^{-3} was employed in these experiments. The influence of ΔP on the residual TiO_2 levels in the bulk feed is more dominant at low values of the cross-flow velocity or shear rate. However, in the high u regime, the deposition of TiO_2 (i.e., gel formation) is inhibited and ΔP plays less of a role in affecting the TiO_2 levels in the bulk feed. It is noteworthy that about 50% of the initial TiO_2 amount can be accumulated at the membrane surface at an (unfavorable) combination of low u and high ΔP.

Table 2. Values of R and J_g at various cross-flow velocities*

Cross-flow velocity /m s^{-1}	R /m^{-1}	J_g /m s^{-1}
0.54	6.36×10^{11}	–
0.97	7.76×10^{11}	1.47×10^{-3}
1.50	7.34×10^{11}	1.56×10^{-3}
2.03	7.23×10^{11}	1.56×10^{-3}
2.92	7.40×10^{11}	–

* See also Figure 6

Table 3. Values of R and J_g at different TiO_2 doses*

TiO_2 dose /g dm^{-3}	R /m^{-1}	J_g /m s^{-1}
0.5	6.71×10^{11}	1.75×10^{-3}
1.0	8.47×10^{11}	1.15×10^{-3}
1.5	8.12×10^{11}	0.55×10^{-3}
2.0	7.55×10^{11}	0.26×10^{-3}
3.0	7.73×10^{11}	0.20×10^{-3}

* See also Figure 7

3.3. *Operation of the integrated photoreactor–UF process assembly*

Table 4 and Figure 8 contain selected data from ten repeat cycles of operation of the integrated assembly. The 20 min dark equlibration time (Section 2) was chosen such that saturation coverage of the TiO_2 surface with the MB dye would have been obtained [1]. Interestingly enough, removal of MB from the solution by the adsorption process *increases* dramatically after the first cycle of operation. A corresponding trend also manifests for the TOC reduction in the dark (Table 4). The mechanistic origins of these trends are being explored in ongoing work.

The photocatalytic treatment was performed for a total period of 35 min (Section 2). In the first cycle of operation, the treatment degraded about 95% of the initial dye. The kinetics data presented in Part I of this series [1] indicate that complete decomposition would have ensued after longer irradiation periods (e.g., 60 min). However, this was not the objective of this study *per se*. Nonetheless, it is interesting to note that further removal of the dye was facilitated by the UF process such that the extent of dye removal was about 98%.

From an environmental perspective, the crucial point to note in the data in Table 4 is that the percent TOC removal after the photocatalysis process in the first cycle was only about 64%. Thus, mineralization of the dye was far from complete and reaction intermediates must account for the residual organic carbon content of the solution. This point has been emphasized by other authors [11, 12]. A small fraction of the residual carbon is removed by the UF process such that the total TOC removal attains about 74%.

Subsequent cycles of operation bring about a systematic degradation in the performance of the photocatalysis (Table 4 and Figure 8). In fact, only a total of about 86% of the dye is removed by the combined photocatalysis–UF process after ten repeat cycles. The corresponding TOC removal was only about 42%.

We suspect that 'caking' of the TiO_2 photocatalyst during the UF process and the subsequent redispersion stage promotes agglomeration of the TiO_2 particles. This results in a progressive diminution in their photocatalytic activity. This notion is supported by the

Table 4. Data from repeat cycles of operation of the integrated photoreactor–UF process assembly

Analysis method	Description	Run number			
		1	*4*	*7*	*10*
UV–VIS spectroscopy	[MB] initial	6.948*	7.274	7.353	7.182
	[MB] after dark reaction	6.782*	6.088	6.059	6.086
	[MB] after photoreaction	0.361*	0.351	1.021	1.422
		94.67**	94.24	83.15	76.63
	[MB] after filtration	0.158*	0.296	0.659	1.034
	Overall [MB] removal	97.73**	95.94	91.04	85.60
TOC	TOC initial	4.200*	4.600	4.900	4.300
	TOC after dark reaction	3.900*	3.800	4.100	3.900
	TOC after photoreaction	1.400*	1.900	2.000	2.800
		64.10**	50.00	51.20	28.21
	TOC after filtration	1.100*	–	1.400	2.500
	Overall TOC removal	73.81**	–	71.43	41.86

* Concentration of MB or TOC (mg dm^{-3})
** Percentage removal (%)

dynamic laser light scattering data presented below. Incorporation of an ultrasonication device in the integrated assembly would be an effective approach to this agglomeration problem.

3.4. *Turbidity and dynamic laser light scattering data*

Turbidity measurements were performed before and after the UF process to assess the extent of removal of the TiO_2 particles from the feed slurry. The removal of TiO_2 was complete in all the cases tested in this study, attesting to the effectiveness of the particular hollow-fibre membrane cartridge that was employed. From an initial turbidity of about 5200 NTU (corresponding to a TiO_2 dose of 1 g dm^{-3}, see Equation 5), the permeate turbidity dropped to the 0.22–0.42 NTU range.

Figure 9 contains turbidity data before and after the combined system operation for ten repeat cycles. The permeate turbidity was down to the 0.26–0.45 NTU level from the initial turbidity in the 5000–6500 NTU range of the suspension. We interpret these data to again signal complete separation of the TiO_2 particles from the slurry feed. Comparison of these data with those in Table 4 and Figure 8 indicate that the TiO_2 particles were the major contributors to the solution turbidity. Neither the initial dye nor the reaction intermediate(s) appear to play a significant role, although there is a slight increase in the turbidity after the fourth repeat cycle.

In an effort to understand the causal factor(s) in the degradation of the photocatalyst performance (Figure 8), the initial particle size distribution in the TiO_2 slurry was compared with the corresponding one after the tenth repeat cycle. Figure 10 contains data obtained from dynamic laser light scattering. Compared to the initial distribution in Figure 10(a), the particle size

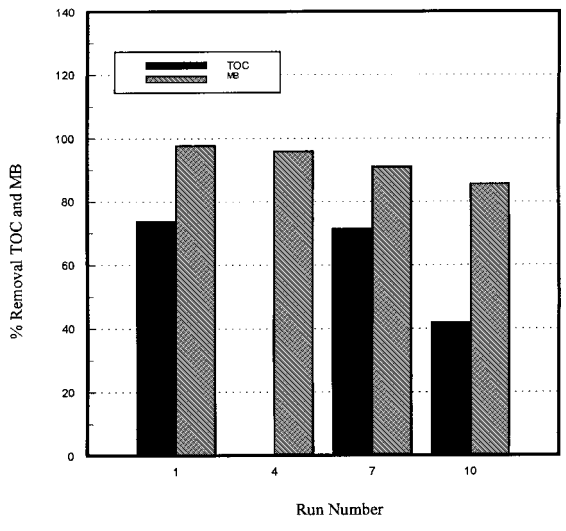

Fig. 8. Removal of MB (as monitored spectrophotometrically) and TOC for the first, fourth, seventh and tenth cycle of operation of the combined system.

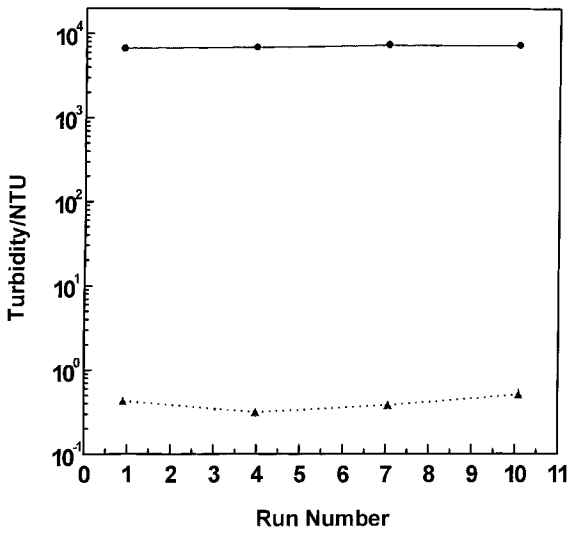

Fig. 9. Turbidity of the solutions initially dosed with 1 g dm^{-3} TiO_2 before and after use in the combined system. As in Figure 8, data are shown for the first, fourth, seventh and tenth cycle of operation. Lines are simply drawn through the data points.

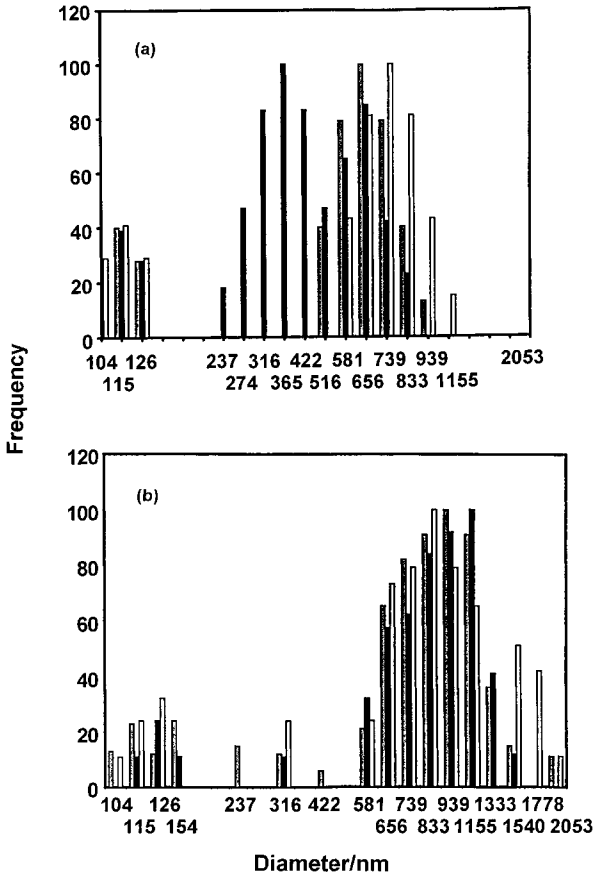

Fig. 10. Dynamic laser light scattering data on a TiO_2 suspension before (Figure 10(a)) and after (Figure 10(b)) use in the combined system. In the latter case, the suspension was after the tenth cycle of operation. Three replicate data sets are shown in each case in histogram format for the particle size distribution.

distribution has shifted to a coarser range (Figure 10(b)) after ten repeat cycles of use. This is consistent with agglomeration of the TiO_2 particles with repeated use in the integrated assembly.

In summation, this study has demonstrated the viability of combining a batch-recirculated photoreactor with a hollow-fibre membrane UF unit for practical implementation of slurry-based heterogeneous photocatalysis. Several important challenges remain, however. The problem of incomplete mineralization of toxic organic compounds (such as MB) by this treatment process, while not unique to the combined approach, must nonetheless be tackled in the future. The systematic degradation in the performance of the combined system with each repeat cycle, as noted in this study, must be suitably addressed. Approaches to this problem based on *in situ* ultrasonification and/or shock-loading during the UF process are being considered in these laboratories.

Acknowledgements

This study was funded, in part, by a subcontract from the National Renewable Energy Laboratory (Subcontract XCK 0-5-14318-03). K. S. thanks the Royal Government of Thailand for leave and financial support to undertake this dissertation work at the University of Texas at Arlington. We thank Professor Z.A. Schelly for access to the dynamic laser light scattering instrument, Dr. B .Derecskei for assistance with these experiments, and the City of Arlington for the TOC analyses. Finally, we acknowledge the invaluable help of Drs C.R. Chenthamarakshan and N.R. de Tacconi in data analysis and Ms. G. Madden in the preparation of this manuscript, respectively.

References

1. K. Sopajaree, S.A. Qasim, S. Basak and K. Rajeshwar, *J. Appl. Electrochem.* **29** (1999) 535–539.
2. M. Mulder, 'Basic Principles of Membrane Technology' (Kluwer Academic, Amsterdam, 1989).
3. M. Cheriyan, *in* 'Ultrafiltration Handbook' (Technomic Publishing Company, Lancaster, PA, 1986), chapter 4, pp. 73–125.
4. A.G. Fane, *J. Membrane Sci.* **20** (1984) 249.
5. A.G. Fane, C.J.D. Fell and A.G. Waters, *J. Membrane Sci.* **9** (1981) 245.
6. B. Chu, 'Laser Light Scattering' (Academic Press, New York, 1974).
7. 'Standard Methods for the Examination of Water and Wastewater' (American Public Health Association, Washington, DC, 18th edn. 1992).
8. K.L. Jones, E.S. Odderstol, G.E. Walterau and M.M. Clark, *J. Amer. Water Works Assoc.*, Oct. (1993) 87.
9. H-M. Yeh and T-W. Chang, *Sep. Sci. Technol.* **29** (1994) 497.
10. H-M. Yeh, *Sep. Sci. Technol.* **31** (1996) 201.
11. C. Minero, E. Pelizzetti, P. Pichat, M. Sega and M. Vincenti, *Environ. Sci. Technol.* **29** (1995) 2226 and references therein.
12. D. Mas, T. Hisanaga, K. Tanaka and P. Pichat, *Trends Photochem. Photobiol.* **3** (1994) 467.